



Oscillons, solitons, and domain walls in arrays of nonlinear plasmonic nanoparticles

Roman Noskov¹, Pavel Belov¹ & Yuri Kivshar^{1,2}

¹National Research University of Information Technologies, Mechanics and Optics (ITMO), St. Petersburg 197101, Russia, ²Nonlinear Physics Center, Research School of Physics and Engineering, Australian National University, Canberra ACT 0200, Australia.

SUBJECT AREAS:

SOLITONS

NANOPHOTONICS AND
PLASMONICS

NANOPARTICLES

STATISTICAL PHYSICS,
THERMODYNAMICS AND
NONLINEAR DYNAMICS

Received
15 October 2012

Accepted
26 October 2012

Published
20 November 2012

Correspondence and
requests for materials
should be addressed to

R.N. (nanometa@
gmail.com)

The study of metal nanoparticles plays a central role in the emerging novel technologies employing optics beyond the diffraction limit. Combining strong surface plasmon resonances, high intrinsic nonlinearities and deeply subwavelength scales, arrays of metal nanoparticles offer a unique playground to develop novel concepts for light manipulation at the nanoscale. Here we suggest a novel principle to control localized optical energy in chains of nonlinear subwavelength metal nanoparticles based on the fundamental nonlinear phenomenon of modulation instability. In particular, we demonstrate that modulation instability can lead to the formation of long-lived standing and moving nonlinear localized modes of several distinct types such as bright and dark solitons, oscillons, and domain walls. We analyze the properties of these nonlinear localized modes and reveal different scenarios of their dynamics including transformation of one type of mode to another. We believe this work paves a way towards the development of nonlinear nanophotonics circuitry.

Modulation instability (MI) is a nonlinearity-induced phenomenon that can be observed in many different branches of physics¹. Due to MI, small noise-driven amplitude and phase perturbations rapidly boost under the influence of nonlinearity and diffraction (or dispersion). Consequently, broad optical beams (or quasicontinuous wave pulses) decay into optical filaments (or pulse trains)^{2–5}. MI also shows up in the pattern formation from noise for partially spatially incoherent light beams propagating through noninstantaneous nonlinear media⁶. Finally, MI development in granular and liquid media is often associated with generation of nonlinear localized states in the form of oscillons (or oscillating solitons) and domain walls^{7–9}. Hopefully, consideration of such intriguing phenomena in plasmonic systems such as metallic nanowires or nanoparticle arrays may open novel routes for light control at the deeply subwavelength structures.

Owing to the ability to squeeze light into a nanometer size regime, surface plasmons supported by noble metal nanostructures are exploited in a huge number of applications ranging from photonic nanocircuitry to biological sensors^{10,11}. However, another remarkable property of noble metals - extremely high intrinsic nonlinearity - remained obscure for a long time because of their natural optical opaqueness. Following in the footsteps of ground-breaking works on a cubic susceptibility of metal colloids^{12–14}, recent advances in the development of high-quality nanostructured systems manifest how to engineer the field penetration inside the nanostructure to fully use its nonlinear response¹⁵. In this context, one may mention optical limiting and self-phase modulation in arrays of structured nanoparticles¹⁶, second and third harmonic generation in nanostructured metal films and nanoantennas^{17–21}, subwavelength solitons in metal-dielectric multilayers^{22–24} and arrays of metal nanowires²⁵, plasmonic kinks and oscillons in nanoparticle arrays^{26,27}, ultrafast all-optical switching in metallic photonic crystals²⁸ as well as metal-semiconductor and metal-dielectric nanoantennas^{29–31}, generation of THz radiation from silver nanodimers^{32,33}, and a nanoradar with periodically rotating scattering pattern³⁴.

Here we present a comprehensive study of MI in subwavelength nonlinear systems for a chain of optically driven metallic nanoparticles with a Kerr-like nonlinear response. We demonstrate the existence of novel types of nonlinear effects in such systems, including generation of domain walls (or switching waves) as well as long-lived standing and moving nonlinear localized modes in the form of bright and dark oscillons and solitons. We reveal that a wide variety of scenarios of MI development allows for the mode transformation from one type to another,



changing the propagation direction and a velocity of drifting oscillons, solitons, and domain walls as well as the formation of stable domain walls connecting not only different stationary states but also the states with different types of nonlinear dynamics.

Results

Model and governing equations. We consider a chain of identical spherical nanoparticles placed close to each other and embedded into a SiO₂ host medium with a permittivity $\epsilon_h = 2.15$ (see Fig. 1). We assume that the particle radius and the center-to-center spacing are $a = 10$ nm and $d = 30$ nm, respectively. Ratio a/d satisfies the condition $a/d \leq 1/3$, so that we can employ the point dipole approximation³⁵. Assuming the nanoparticles made of silver with a nonlinear Kerr-like response, we take the dielectric constant in the form $\epsilon_{Ag}^{NL} = \epsilon_{Ag}^L + \chi^{(3)} |\mathbf{E}_n^{(in)}|^2$, where the linear part is given by the Drude formula, $\epsilon_{Ag}^L = \epsilon_\infty - \omega_p^2 / [\omega(\omega - i\nu)]$, with $\epsilon_\infty = 4.96$, $\hbar\omega_p = 9.54$ eV, and $\hbar\nu = 0.055$ eV³⁶, and $\mathbf{E}_n^{(in)}$ is the local field inside the n th particle. In general, the value of the cubic susceptibility for metallic nanoparticles depends on a number of factors, including the type of metal, particle size, external pulse duration and frequency, and others³⁷. However, the analytical quantum model derived in Refs.^{38,39} and confirmed with numerical simulations⁴⁰ and experimental data^{12,14} showed that silver nanoparticles with radius 10 nm and driven at the frequency close to the frequency of the surface plasmon resonance possess a remarkably high and purely real cubic susceptibility $\chi^{(3)} \simeq 3 \times 10^{-9}$ esu. Note fused silica possesses negligibly weak cubic nonlinearity ($\sim 10^{-15}$ esu⁴¹) as well as a good enough optical transparency⁴² to maintain the strong laser powers needed for the observation of MI.

We study a nanoparticle chain driven by an arbitrary optical field with the frequency close to the frequency of the surface plasmon

resonance of an individual particle, and analyze the dynamical response of the particle polarizations, \mathbf{p}_n , through the model proposed in our previous article²⁷, which yields the following system of coupled equations for the slowly varying amplitudes of the particle dipole moments,

$$\begin{aligned} -i \frac{dP_n^\perp}{d\tau} + (-i\gamma + \Omega + |\mathbf{P}_n|^2) P_n^\perp + \sum_{m \neq n} G_{n,m}^\perp P_m^\perp &= E_n^\perp, \\ -i \frac{dP_n^\parallel}{d\tau} + (-i\gamma + \Omega + |\mathbf{P}_n|^2) P_n^\parallel + \sum_{m \neq n} G_{n,m}^\parallel P_m^\parallel &= E_n^\parallel, \end{aligned} \quad (1)$$

where

$$\begin{aligned} G_{n,m}^\perp &= \frac{\eta}{2} \left((k_0 d)^2 - \frac{ik_0 d}{|n-m|} - \frac{1}{|n-m|^2} \right) \frac{e^{-ik_0 d|n-m|}}{|n-m|}, \\ G_{n,m}^\parallel &= \eta \left(\frac{ik_0 d}{|n-m|} + \frac{1}{|n-m|^2} \right) \frac{e^{-ik_0 d|n-m|}}{|n-m|}, \end{aligned}$$

$P_n^{\perp,\parallel}$ and $E_n^{\perp,\parallel}$ are dimensionless slowly varying amplitudes of the particle dipole moments and external electric field, respectively, the indices ‘ \perp ’ and ‘ \parallel ’ stand for the transverse and longitudinal components with respect to the chain axis, η defines strength of dipole-dipole interaction, $|\mathbf{P}_n|^2 = |P_n^\perp|^2 + |P_n^\parallel|^2$ is a nonlinear term appeared after expressing $\mathbf{E}_n^{(in)}$ via \mathbf{p}_n , γ describes thermal and radiation losses of particles, $k_0 = \omega_0 / c\sqrt{\epsilon_h}$ is the wavenumber of light in a host matrix, $\Omega = (\omega - \omega_0) / \omega_0$, and $\tau = \omega_0 t$ (see Methods). We notice that this model involves all particle interactions through the dipole fields, and it can be applied to both finite and infinite chains.

To begin with, we excite the infinite chain by an electric field with one of the two polarizations: (i) $\mathbf{E}_n = (E_0^\perp \exp(-iQdn), 0)$ and (ii) $\mathbf{E}_n = (0, E_0^\parallel \exp(-iQdn))$, where Q is the wavenumber along the

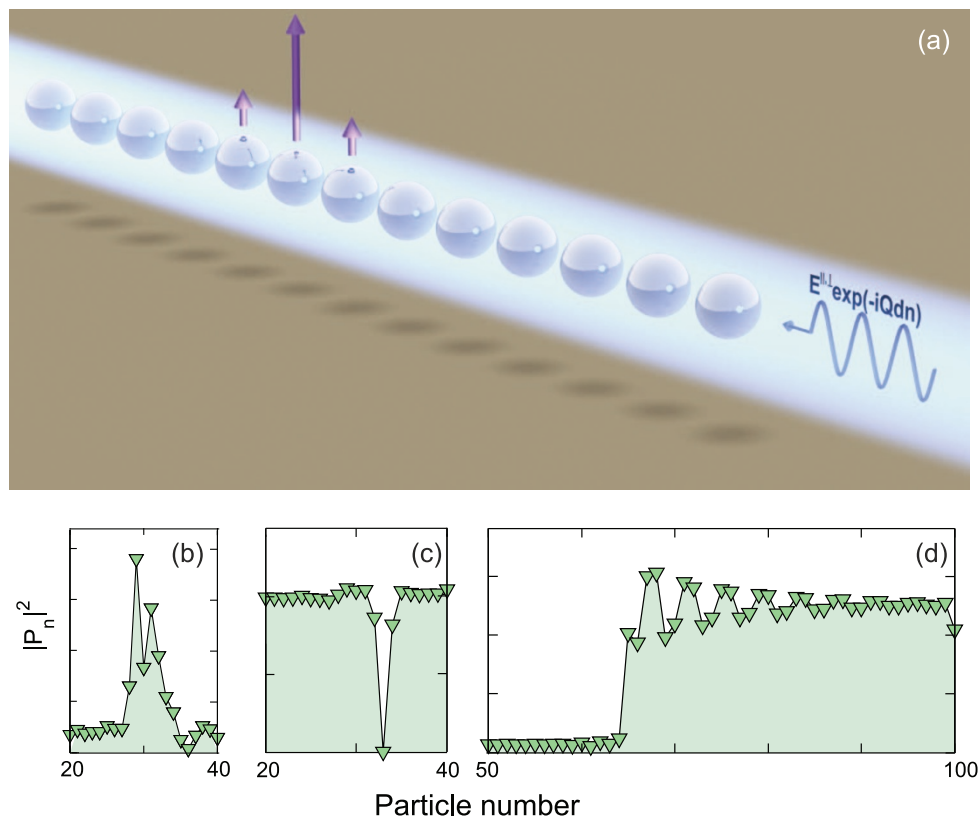


Figure 1 | Schematic of a chain of metallic nanoparticles illuminated by a laser beam and profiles of nonlinear localized states. (a) Arrows indicate particle polarizations for a bright soliton/oscillon. Panels (b), (c) and (d) depict profiles of the polarizations for a typical soliton/oscillon configuration of bright and dark forms as well as domain wall, respectively.



chain axis. We suppose that Q may vary in a wide range, $0 \leq Qd \leq \pi$. In practice $0 < Q < k_0$ can be realized through tilted light incidence on the chain, while $Q > k_0$ can be provided by means of a scheme based on, e.g., total internal reflection, as it was suggested recently for investigation of localized plasmon modes in metallic nanoparticle chains⁴³. The simplest case of homogenous excitation, i.e. $Q = 0$, has been considered earlier²⁷, and we observed periodic pattern formation and generation of oscillons. Below we will show that adjustment of Q opens a wide variety of novel scenarios of MI development.

Spatially modulated external field allows us to treat particle dipole moments as $P_n^{\perp,\parallel} = P_0^{\perp,\parallel} \exp(-iQdn)$. In this case, the system stationary states can be written as follows

$$\left(-i\gamma + \Omega + \sum_{j=1}^{\infty} A_j^{\perp,\parallel} + |P_0^{\perp,\parallel}|^2 \right) P_0^{\perp,\parallel} = E_0^{\perp,\parallel}, \quad (2)$$

where

$$A_j^{\perp} = \eta \left(\frac{(k_0 d)^2}{j} - \frac{ik_0 d}{j^2} - \frac{1}{j^3} \right) \cos(Qdj) \exp(-ik_0 dj),$$

and

$$A_j^{\parallel} = 2\eta \left(\frac{ik_0 d}{j^2} + \frac{1}{j^3} \right) \cos(Qdj) \exp(-ik_0 dj).$$

A transition from $G_{n,m}^{\perp,\parallel}$ to $A_j^{\perp,\parallel}$ has been made via the replacement $|n - m| = j$ and taking into account symmetry structure of the series. This equation has multiple solutions for $\Omega < -\text{Re} \sum_{j=1}^{\infty} A_j^{\perp,\parallel} - \sqrt{3} |\gamma - \text{Im} \sum_{j=1}^{\infty} A_j^{\perp,\parallel}|$ leading to a bistable regime.

Linear stability analysis and numerical simulations of modulation instability. Next, we analyze linear stability of the stationary states (2) with respect to weak spatiotemporal perturbations, and derive the expression for the instability growth rate (see *Methods*),

$$\lambda_{\perp,\parallel} = \tilde{\gamma}_{\perp,\parallel} + \left\{ |P_0^{\perp,\parallel}|^4 - \left(2|P_0^{\perp,\parallel}|^2 + \Omega + \text{Re} \sum_{j=1}^{\infty} B_j^{\perp,\parallel} \right)^2 \right\}^{1/2},$$

where $\tilde{\gamma}_{\perp,\parallel} = \text{Im} \sum_{j=1}^{\infty} B_j^{\perp,\parallel} - \gamma$, $B_j^{\perp,\parallel} = A_j^{\perp,\parallel} \cos(Kdj)$. Thus, the initial nonlinear modulated states (2) become unstable provided $\lambda_{\perp,\parallel} > 0$. The stability depends on the external field parameters $E_0^{\perp,\parallel}$, Ω , and Q as well as on the modulation wavenumber of perturbation, K .

Consider the case of the transversal excitation in detail. Figure 2(a) shows regions of MI in the plane $(\Omega, |E_0^{\perp}|^2)$ obtained from the condition $\lambda_{\perp} = 0$ at any K and $Qd = 0.7$ that corresponds to grazing incidence of light at the angle 2.5° relative to the chain axis. Importantly, external field modulation results in the remarkable fact that the MI development can be reached with respect to both fast (with $K < k_0$) and slow (with $K > k_0$) system eigenmodes in contrast to the case of homogeneous excitation, for which MI generation is achievable with respect to slow eigenmodes only²⁷. The first possibility opens a promising perspective for dynamical engineering of the chain scattering pattern similar to nanoradar³⁴; whereas the second provides the straightforward rote for manipulation of strongly localized nonlinear states. In this work we focus on the latter approach.

Contour maps of λ_{\perp} in the planes $(Kd, |E_0^{\perp}|^2)$ and (Qd, Kd) are presented in Figs. 2(b) and 2(c), respectively. As follows from these figures, one can generate MI within either slow or fast eigenmodes by proper adjustment of $|E_0^{\perp}|^2$ and Q , enabling dynamical transformation of free propagating radiation into a nonlinear localized form and vice versa, a localized external excitation into free propagating radiation. These possibilities correspond to the zones with $K > k_0$, $Q < k_0$ and $K < k_0$, $Q > k_0$ in Fig. 2(c), respectively.

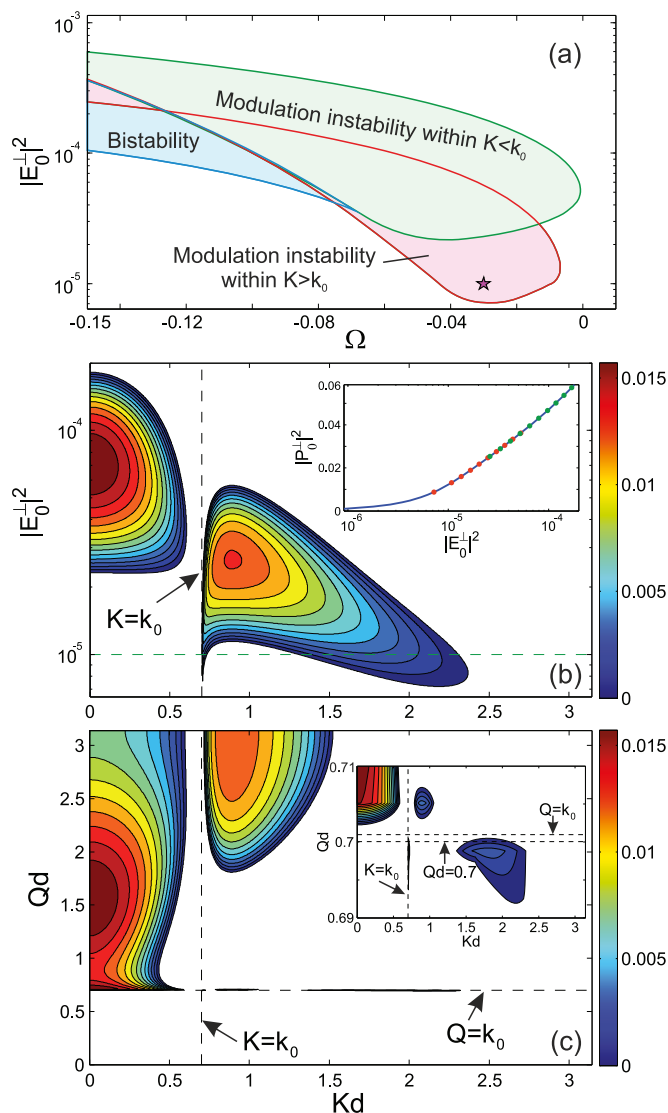


Figure 2 | Bifurcation diagram and contour maps of the instability growth rate at the transversal excitation. (a) Bifurcation diagram on the parameter plane of $\Omega = (\omega - \omega_0)/\omega_0$ and $|E_0^{\perp}|^2$ and $Qd = 0.7$, with the regions of bistability (blue) and modulation instability (green and red). Red and green zones correspond to MI development relative to slow (with $K > k_0$) and fast (with $K < k_0$) eigenmodes of the chain, respectively. The purple star denotes intensity $|E_0^{\perp}|^2 = 10^{-5}$ (which is also marked by the horizontal dashed line in (b)) and frequency $\Omega = -0.03$ used for drawing contour maps of λ_{\perp} on the planes (b) $(Kd, |E_0^{\perp}|^2)$ and (c) (Kd, Qd) as well as in numerical simulations of Eq. (1) shown in Fig. 3. Inset in (b) demonstrates dependence of the polarization $|P_0^{\perp}|^2$ on $|E_0^{\perp}|^2$ for $\Omega = -0.03$. Red and green dots indicate red and green zones of modulation instability from (a), respectively. Inset in (c) shows the enlarged contour map of λ_{\perp} in the vicinity of $Qd = 0.7$.

In order to examine the spatiotemporal evolution of the chain beyond the instability point, we perform numerical simulations of Eq. (1) for a finite chain (with 100 nanoparticles) at zero initial conditions, when the external field increases slowly approaching to the saturation level E_0^{\perp} , which is reached at $\tau \approx 100$. We selected $|E_0^{\perp}|^2 = 10^{-5}$, $\Omega = -0.03$ and $Q = 0.7$ to undergo MI out of the bistability zone and with respect to slow eigenmodes only (see Figs. 2(a), (b), and (c)). Edge effects acted as small perturbations needed for MI onset.

The result is presented in Fig. 3, where we observe that instability provokes formation of a train of bright oscillons. Oscillons appear at

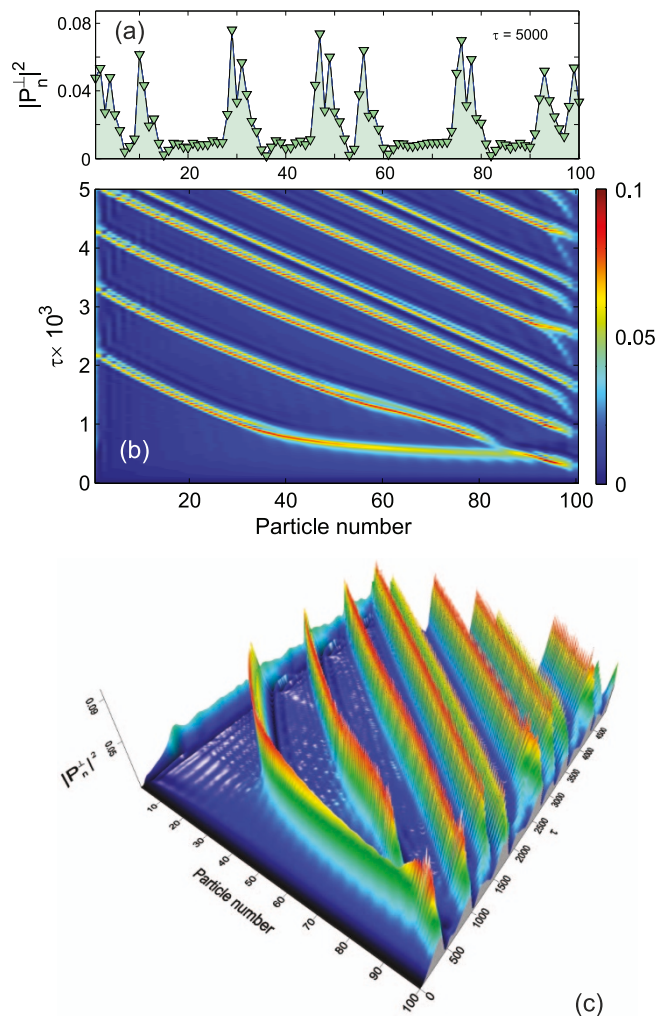


Figure 3 | Train of bright oscillons. Dynamics of the particle polarizations $|P_n^\perp|^2$ obtained by numerical simulations of Eq. (1) at $\Omega = -0.03$, $|E_0^\perp|^2 = 10^{-5}$, and $Qd = 0.7$, when the light beam propagating at the angle 2.5° with respect to the chain axis provokes generation of a train of bright oscillons. Panel (a) shows a snapshot of $|P_n^\perp|^2$ at $\tau = 5000$. Panels (b) and (c) represent 2D and 3D views of the spatiotemporal dynamics of $|P_n^\perp|^2$, respectively. See also *Supplementary Material* for the associated time animations of particle polarizations.

the right side of the chain and move with the speed $\sim 0.013c$ in the opposite direction with respect to the direction of light propagation, as shown in Fig. 1. Having reached the left side of the chain, they transform into free propagating radiation, and a small part of energy is reflected back in the chain, eventually decaying. We notice this type of oscillons is generated in a two-pick form, and the first oscillon turned into an oscillon and a soliton, which later transformed back into an oscillon. Remarkably, all bright oscillons are localized on 7 particles, and their width is about 210 nm.

Next, we conduct the similar analysis for the case of the longitudinal excitation. Figures 4(a) to (c) show the corresponding bifurcation diagram and contour maps. In contrast to the transversal case, the MI growth of both localized (with $Q > k_0$) and free propagating (with $Q < k_0$) excitations can be reached within slow eigenmodes only. Since the instability growth rate takes the maximum values for modes with $Kd \sim \pi$, one may expect that the subsequent evolution of the unstable system will lead to formation of a high-order mode.

Indeed, numerical simulations confirm appearance of small-amplitude high-order modulations, but accompanied by an array of standing dark solitons, as shown in Figs. 5 (a) and (b).

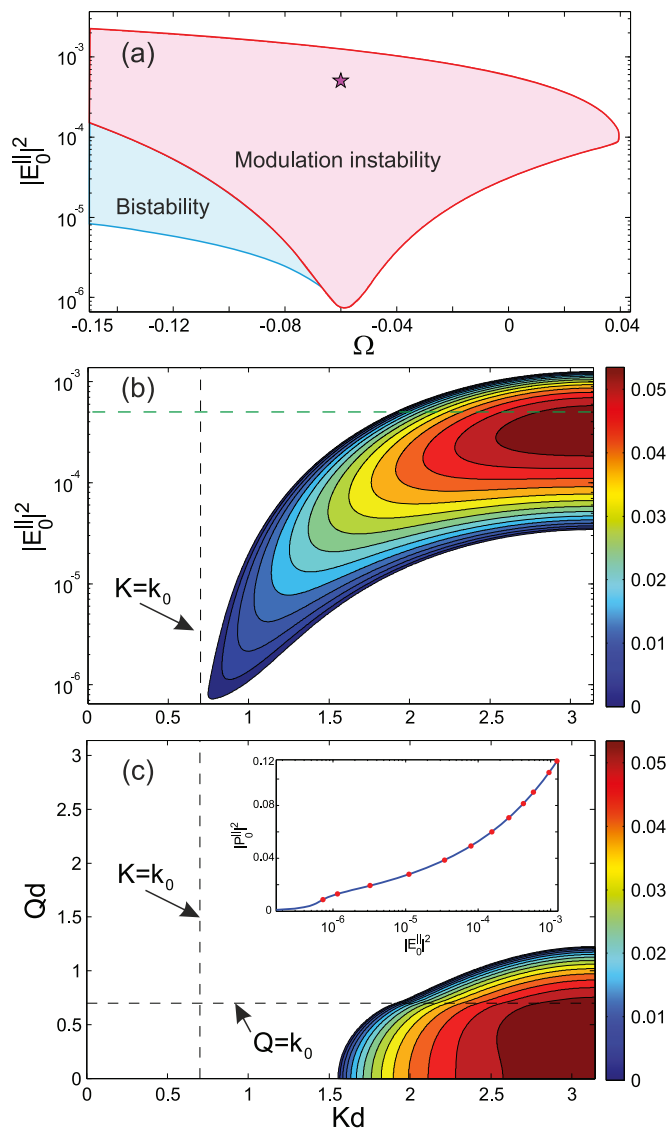


Figure 4 | Bifurcation diagram and contour maps of the instability growth rate at the longitudinal excitation. (a) Bifurcation diagram at $Qd = 0.7$. The purple star denotes intensity $|E_0^\perp|^2 = 5 \times 10^{-4}$ (which is also marked by the horizontal dashed line in (b)) and frequency $\Omega = -0.06$ used for drawing contour maps of $\lambda_{||}$ on the planes (b) $(Kd, |E_0^\perp|^2)$ and (c) (Kd, Qd) as well as in numerical simulations of Eq. (1) shown in Figs. 5 (a) and (b). Inset demonstrates dependence of the polarization $|P_0^\perp|^2$ on $|E_0^\perp|^2$ for $\Omega = -0.06$. Red dots indicate the area of MI.

Surprisingly, despite long-range interactions, all these solitons are localized only on 1 particle. Nevertheless, nonlocality of particle interaction is manifested in a soliton-to-soliton distance which varies between 8 and 12 particles in the middle of the chain and decreases to 2–6 nanoparticles close to the edges.

In addition to dark solitons, we observed generation of standing dark oscillons, as shown in Figs. 6(a) and (b). They also are localized on 1 particle, but with a flat background. Although MI growth leads to formation of dark oscillons along all the chain, only 3 of them eventually remain stable; while others decay. Therefore, one may conclude that in general standing dark oscillons are less stable than standing dark solitons.

Figures 6 (c) and (d) represent a train of dark oscillons. Similar to drifting bright oscillons, drifting dark oscillons are generated at the right edge of the chain and move with the starting velocity $0.014c$,

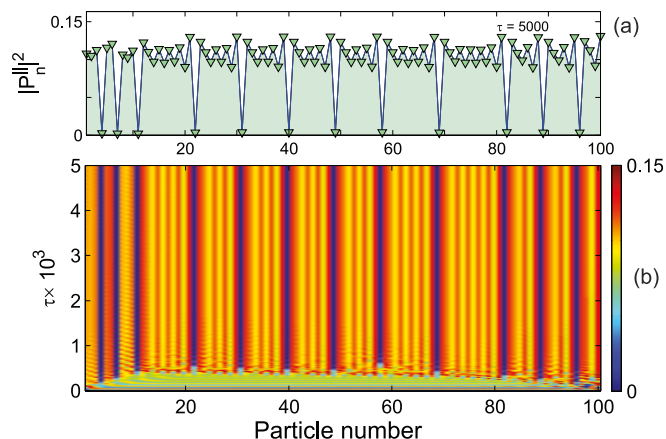


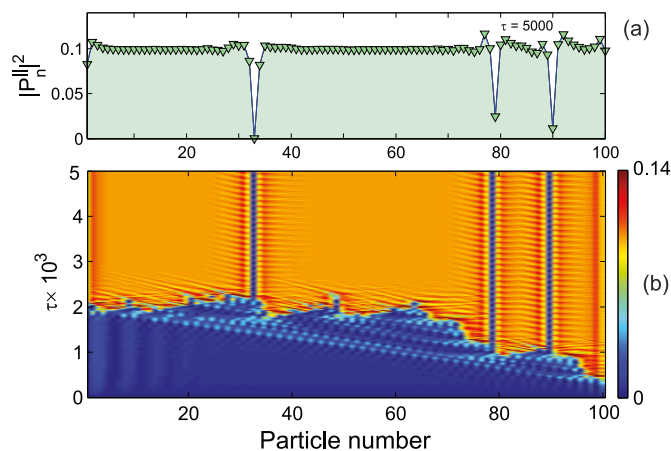
Figure 5 | Dark solitons observed in the longitudinally excited chain at $\Omega = -0.06$, $|E_0^||^2 = 5 \times 10^{-4}$, $Qd = 0.7$. Panel (a) shows a snapshot of the particle polarizations $|P_n^||^2$ at $\tau = 5000$; while panel (b) represents a 2D view of the spatiotemporal dynamics of $|P_n^||^2$. See also *Supplementary Material* for the associated time animation.

slowly decelerating. Then they collapse or stay (not shown) on the way, not reaching the other side. Interestingly, this kind of oscillons combines a narrow width about 3 particles (apart from the first oscillon whose width varies from 11 to 3 particles) with quite a long tail consisting 11 particles.

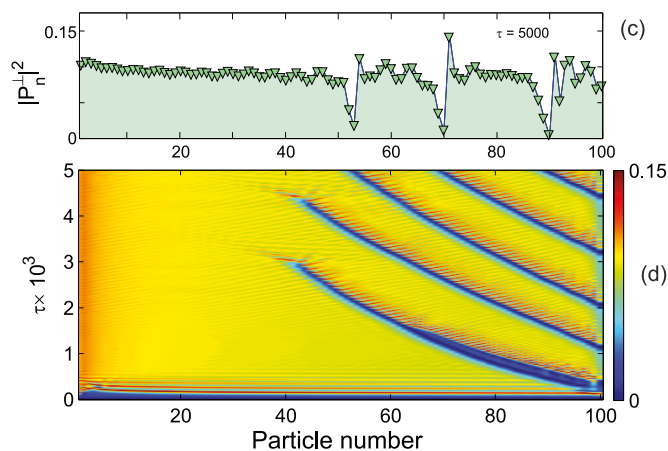
The important property of oscillons is the ability to change the movement direction. That case is presented in Figs. 6 (e) and (f), where the walking oscillon in a high-contrast background is slow drifting along the chain, switching the movement direction from time to time. Remarkably, the absolute value of the velocity remains constant and equals to $0.0037c$. While this simulation shows only the oscillon which walks around the middle of the chain, other scenarios of MI development with close parameters allow arrest of the walking oscillon by the edge and subsequent transformation into the surface localized state (not shown).

Domain walls. Finally, we analyze domain walls (or switching waves). In general there are two mechanisms leading to domain wall formation: bistability and modulation instability. Bistability-induced domain walls also often referred as kinks connect two different stable states of particle polarizations. MI makes twofold

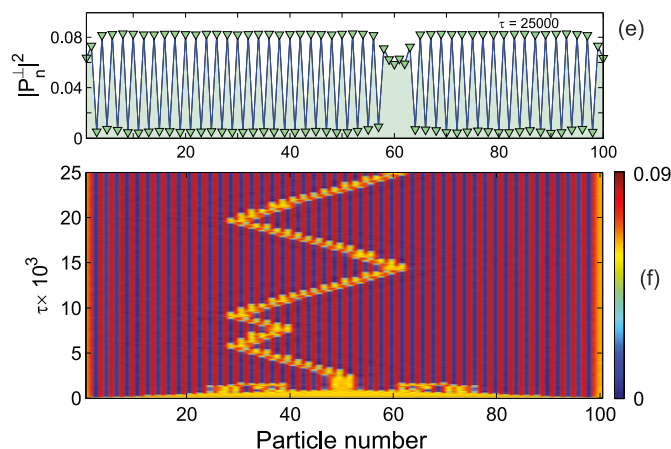
Dark oscillons



Train of dark oscillons



Walking grey oscillon



Domain wall

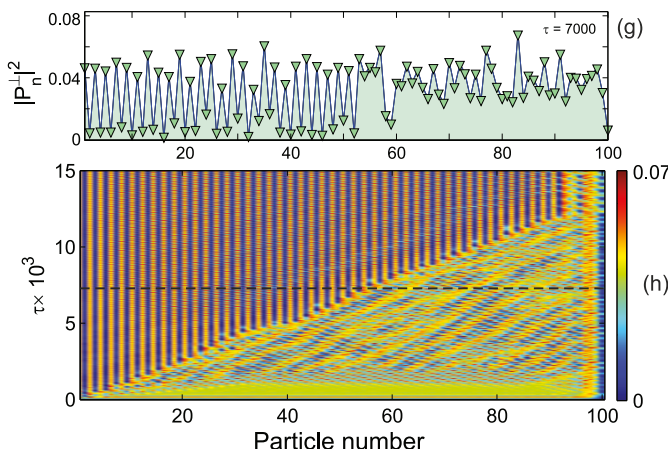


Figure 6 | Examples of nonlinear localized states. Panels (a,b) indicate generation of dark oscillons in the longitudinally excited chain at $\Omega = -0.05$, $|E_0^||^2 = 4.5 \times 10^{-5}$, $Qd = 2$. Panels (c,d) show a train of dark oscillons in the transversally excited chain at $\Omega = -0.06$, $|E_0^||^2 = 1.2 \times 10^{-4}$, $Qd = 0.7$. Panels (e,f) represent the case of the oscillon with a changeable direction of movement but the constant absolute value of the speed $\sim 0.0037c$ in the transversally excited chain at $\Omega = -0.0475$, $|E_0^||^2 = 7 \times 10^{-5}$, $Qd = \pi$, respectively. Panels (g,h) demonstrate formation of the domain wall between parts of the chain with regular and chaotic-like dynamics. The horizontal dashed line in (h) marks a time moment for the frozen frame shown in (g). See also *Supplementary Material* for the associated time animations.



impact with respect to domain walls. When MI occupies at least one of the bistability branches, domain walls generation typically cannot be realized. For instance, this case corresponds to the bifurcation diagrams shown in Figs. 2 (a) and 4 (a). On the other hand, MI is able to generate domain walls beyond the bistability regime on its own. Figures 6 (g) and (h) demonstrate an example of such a domain wall which appeared between the states with high-order modulations, accompanied by small amplitude beatings, and a chaotic-like behavior. Having appeared at the left edge, such a switching wave drifts with a variable velocity until stay close to the other side. Interestingly, domain wall stopping results in changing chaotic-like dynamics with regular beatings.

In our previous work²⁷ we showed that in the case of homogenous transversal excitation MI occupies only a small region of intensities close to the upper threshold of the bistability area, making possible kink generation. For that case we also observed kinks with zero velocity and one-way movement²⁶. Here we extend our analysis further and reveal switching the kink velocity from negative to positive values. The velocity sign is defined positive if the motion of the switching wave leads to the expansion of the region occupied by the upper branch of bistability; otherwise, the velocity is negative.

To observe kink dynamics, we perform numerical simulations of Eq. (1) for a finite array (with 200 nanoparticles) at initial conditions corresponding to different branches of the homogeneous stationary solution (2) over different parts of the array. Light intensity is supposed to be a step-like function of time, as shown in Fig. 7 (a). Constant E_0^\perp results in the constant kink velocity, v . That is why a step-like time dependency of E_0^\perp allows us to control v .

The results are presented in Fig. 7 (b) where the kink velocity is switched from negative to positive values, passing through zero. A rigorous analysis manifests that there is no smooth transition between kinks with negative, positive, and zero velocities, as shown in Fig. 7 (c). Moreover, these states possess different structures: kinks with positive and zero velocities demonstrate zero width; while the width of kinks with negative velocity extends for 12 particles. We also notice that negative-velocity kinks exist for the same intensities as

stationary (zero-velocity) kinks do. Therefore, to provoke domain wall moving in the negative direction one should force the dipole next to the domain wall into the lower branch of the bistability band until the domain wall starts moving. An opposite transition can be realized through only variation in the intensity, as shown in Fig. 7 (c).

Discussion

The above examples demonstrate how modulation instability and bistability can be used to manipulate light in arrays of nonlinear plasmonic nanoparticles coupled through all dipole fields. In particular, we revealed the generation of long-lived standing and moving nonlinear localized modes in the form of plasmonic oscillons and solitons of both bright and dark types as well as plasmonic domain walls.

Notably, formation of solitons/oscillons can be predominantly governed by either short-range or combination of short-range and long-range interactions. This is best illustrated in localization ranging from 1 to 11 nanoparticles that answers the dimensional scales from 0.05λ to 0.8λ , because $\Omega \ll 1$ corresponds to the radiation wavelength $\lambda \sim 400$ nm.

Long-range interaction also features in kink dynamics. Addressing to a similar model applied to investigation of kinks in arrays of splitting resonators coupled only through near field^{44,45}, we find that long-range interaction splits branches with positive and zero velocities for $v(|E_0^\perp|^2)$ and extends the range of intensities for stationary kinks to the lower threshold of the bistability area. In addition, a near-field model does not distinguish the structure of the kinks with positive and negative velocities; while our model taking into account coupling via all dipole fields indicates a dramatic change in kink width when the velocity sign is changed (see above).

It may be of interest to compare MI-induced plasmon solitons/oscillons in nanoparticle chains with plasmon solitons supported by metal-dielectric multilayered structures²² and arrays of metallic nanowires²⁵. All these nonlinear localized states demonstrate subwavelength localization. However, solitons in 1D multilayers and 2D nanowire lattices extend for 0.3λ and 0.6λ , respectively; whereas the width of solitons/oscillons in nanoparticle chains may reach 0.05λ .

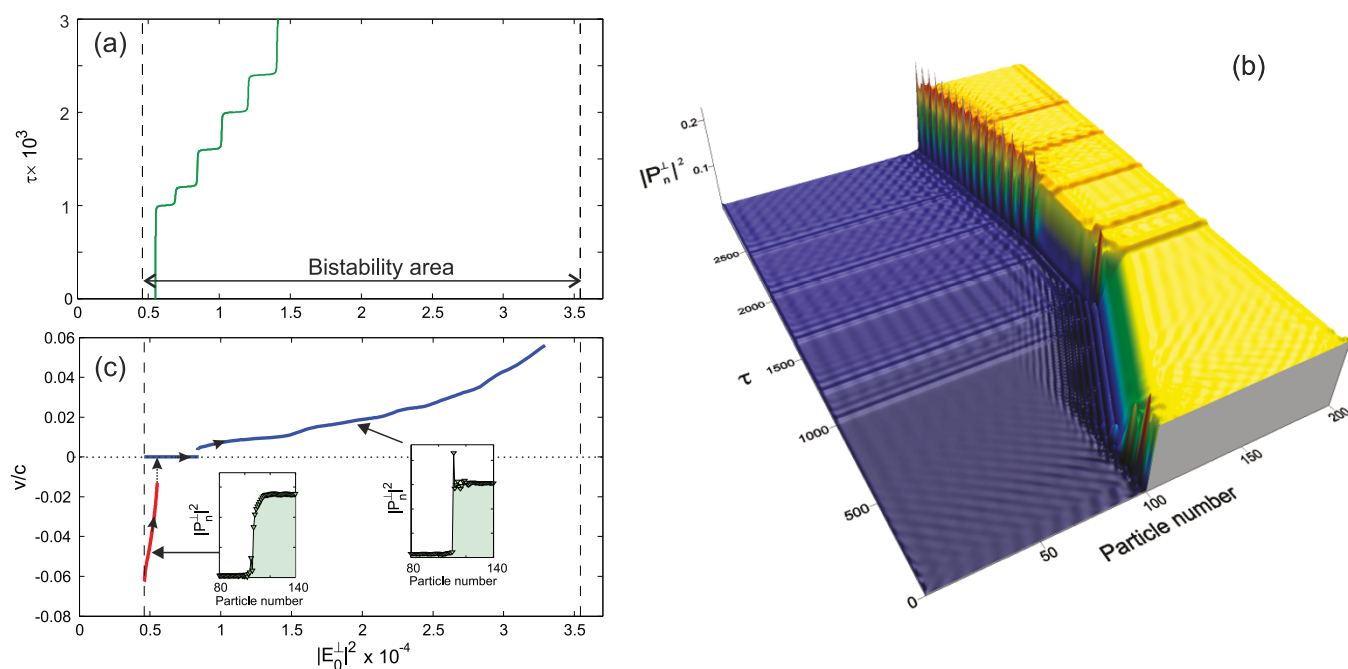


Figure 7 | Control over the kink velocity. Panel (a) demonstrates stimuli vs. time resulting in spatiotemporal dynamics of a kink (switching wave), shown in (b) ($\Omega = -0.1$, $Q = 0$). Panel (c) indicates the normalized kink velocity vs. the intensity of the applied field. A blue curve does not reach the upper threshold of the bistability area because kinks do not exist here owing to MI. Insets show kink structures with positive and negative velocities. See also *Supplementary Material* for the associated time animation.



Besides, MI may create dark solitons/oscillons which were never studied before for plasmonic systems. Thus, MI in arrays of plasmonic nanoparticles opens a perspective way for generation of extremely squeezed nonlinear localized states unreachable with other nonlinear plasmonic structures.

It is also insightful to estimate the maximal pulse duration, because the saturation intensity of the external field $|E_0^{\perp,\parallel}|^2 \sim 10^{-4} - 10^{-5}$, corresponded to the intensity of $\sim 1 - 10$ MW/cm², can lead to thermal damage. Using the value of the ablation threshold of 3.96 J/cm² obtained for silver particles in a SiO₂ host matrix in the picosecond regime of illumination⁴⁶ and taking into account the amplification of the electric field inside the Ag nanoparticle due to surface plasmon resonance, we evaluate the maximal pulse duration as 5 ns for the intensity 0.75 MW/cm² ($|E_0^{\perp,\parallel}|^2 = 10^{-5}$), required for generation of a train of bright oscillons. Since a typical interval between formation of oscillons is about 150 fs ($\Delta\tau \simeq 700$), one may observe generation of ~ 33000 oscillons before a chain will be destroyed. Figures 5 to 7 show similar characteristic times for other nonlinear localized states and domain walls. Therefore, all predicted phenomena can be readily observed in experiment.

Our findings provide a starting platform for further experimental studies of the nonlinearity-induced instabilities and associated phenomena in plasmonic nanostructures which could have important implications for active nanophotonic devices operating beyond the diffraction limit.

Methods

In our theoretical analysis, we use following dimensionless quantities

$$P_n^{\perp,\parallel} = \frac{\sqrt{\chi^{(3)}} P_n^{\perp,\parallel}}{\sqrt{2(\epsilon_{\infty} + 2\epsilon_h)\epsilon_h a^3}},$$

$$E_n^{\perp,\parallel} = \frac{-3\epsilon_h \sqrt{\chi^{(3)}} E_n^{(ex)\perp,\parallel}}{\sqrt{8(\epsilon_{\infty} + 2\epsilon_h)^3}},$$

$$\eta = \frac{3\epsilon_h}{\epsilon_{\infty} + 2\epsilon_h} \left(\frac{a}{d}\right)^3, \quad \gamma = \frac{v}{2\omega_0} + (k_0 a)^3 \frac{\epsilon_h}{\epsilon_{\infty} + 2\epsilon_h}.$$

To derive the instability growth rate, we utilized the standard technique⁴⁷, and take the small perturbations in the form of chain eigenmodes:

$\delta P_n^{\perp,\parallel} = A_{\perp,\parallel} \exp(-iK dn + \lambda_{\perp,\parallel} \tau) + A_{\perp,\parallel}^* \exp(iK dn + \lambda_{\perp,\parallel}^* \tau)$, where ‘*’ means complex conjugation, K is the modulation wavenumber, $A_{\perp,\parallel}$ are amplitudes of perturbation. Having substituted $P_n^{\perp,\parallel} = P_0^{\perp,\parallel} \exp(-iQdn) + \delta P_n^{\perp,\parallel}$ into Eq. (1), we come to the expression for the instability growth rate.

Numerical simulations of Eq. (1) were performed by means of a commercial package Matlab v. 7 with a fourth-order Runge-Kutta scheme, and relative and absolute error tolerances were fixed as 10^{-4} and 10^{-6} , respectively.

- Zakharov, V. & Ostrovsky, L. Modulation instability: The beginning. *Physica, D* **238**, 540 (2009).
- Bespalov, V. I. & Talanov, V. I. Filamentary structure of light beams in nonlinear liquids. *JETP Lett.* **3**, 307 (1966).
- Karpman, V. I. Self-modulation of nonlinear plane waves in dispersive media. *JETP Lett.* **6**, 277 (1967).
- Hasegawa, A. & Brinkman, W. F. J. Tunable coherent IR and FIR sources utilizing modulational instability. *Quant. Electron.* **16**, 694 (1980).
- Agrawal, G. P. Modulation instability induced by cross-phase modulation. *Phys. Rev. Lett.* **59**, 880 (1987).
- Kip, D., Soljacic, M., Segev, M., Eugenieva, E. & Christodoulides, D. N. Modulation instability and pattern formation in spatially incoherent light beams. *Science* **90**, 495 (2000).
- Umbanhowar, P. B., Melo, F. & Swinney, H. L. Localized excitations in a vertically vibrated granular layer. *Nature* **382**, 793 (1996).
- Arbell, H. & Fineberg, J. Temporally harmonic oscillons in Newtonian fluids. *Phys. Rev. Lett.* **85**, 756 (2000).
- Blair, D., Aranson, I. S., Crabtree, G. W., Vinokur, V., Tsimring, L. S. & Josserand, C. Patterns in thin vibrated granular layers: Interfaces, hexagons, and superoscillons. *Phys. Rev. E* **61**, 5600 (2000).
- Pelton, M., Aizpurua, J. & Bryant, G. Metal-nanoparticle plasmonics. *Laser & Photon. Rev.* **2**, 136 (2008).
- Gramotnev, D. K. & Bozhevolnyi, S. I. Plasmonics beyond the diffraction limit. *Nature Photon.* **4**, 83 (2010).

- Ricard, D., Roussignol, P. & Flytzanis, C. Surface-mediated enhancement of optical phase conjugation in metal colloids. *Opt. Lett.* **10**, 511 (1985).
- Hache, F., Ricard, D., Flytzanis, C. & Kreibig, U. The optical Kerr effect in small metal particles and metal colloids: the case of gold. *Appl. Phys. A: Solids Surf.* **47**, 347 (1988).
- Uchida, K., Kaneko, S., Omi, S., Hata, C., Tanji, H., Asahara, Y. & Ikushima, A. J. Optical nonlinearities of a high concentration of small metal particles dispersed in glass: copper and silver particles. *JOSA B* **11**, 1236 (1994).
- Lepeshkin, N. N., Schweinsberg, A., Piredda, G., Bennink, R. S. & Boyd, R. W. Enhanced nonlinear optical response of one-dimensional metal-dielectric photonic crystals. *Phys. Rev. Lett.* **93**, 123902 (2004).
- Panoiu, N. C. & Osgood, R. M. Subwavelength nonlinear plasmonic nanowire. *Nano Lett.* **4**, 2427 (2004).
- Fan, W., Zhang, S., Panoiu, N. C., Abdenour, A., Krishna, S., Osgood, R. M., Malloy, K. J. & Brueck, S. R. J. Second harmonic generation from a nanopatterned isotropic nonlinear material. *Nano Lett.* **6**, 1027 (2006).
- van Nieuwstadt, J. A. H., Sandke, M., Enoch, S. & Kuipers, L. Strong modification of the nonlinear optical response of metallic subwavelength hole arrays. *Phys. Rev. Lett.* **97**, 146102 (2006).
- Klein, M. W., Wegener, M., Feth, N. & Linden, S. Experiments on second- and third-harmonic generation from magnetic metamaterials. *Opt. Express* **15**, 5238 (2007).
- Zhang, Y., Grady, N. K., Ayala-Orozco, C. & Halas, N. J. Three-dimensional nanostructures as highly efficient generators of second harmonic light. *Nano Lett.* **11**, 5519 (2011).
- Butet, J., Russier-Antoine, I., Jonin, C., Lascoux, N., Benichou, E. & Brevet, P.-F. Sensing with multipolar second harmonic generation from spherical metallic nanoparticles. *Nano Lett.* **12**, 1697 (2012).
- Liu, Y., Bartal, G., Genov, D. A. & Zhang, X. Subwavelength discrete solitons in nonlinear metamaterials. *Phys. Rev. Lett.* **99**, 153901 (2007).
- Marini, A., Gorbach, A. V. & Skryabin, D. V. Coupled-mode approach to surface plasmon polaritons in nonlinear periodic structures. *Opt. Lett.* **35**, 3532 (2010).
- Marini, A., Skryabin, D. V. & Malomed, B. Stable spatial plasmon solitons in a dielectric-metal-dielectric geometry with gain and loss. *Opt. Express* **19**, 6616 (2011).
- Ye, F., Mihalache, D., Hu, B. & Panoiu, N. C. Subwavelength plasmonic lattice solitons in arrays of metallic nanowires. *Phys. Rev. Lett.* **104**, 106802 (2010).
- Noskov, R. E., Belov, P. A. & Kivshar, Y. S. Subwavelength plasmonic kinks in arrays of metallic nanoparticles. *Opt. Express* **20**, 2733 (2012).
- Noskov, R. E., Belov, P. A. & Kivshar, Y. S. Subwavelength modulational instability and plasmon oscillons in nanoparticle arrays. *Phys. Rev. Lett.* **108**, 093901 (2012).
- Utikal, T., Hentschel, M. & Giessen, H. Nonlinear photonics with metallic nanostructures on top of dielectrics and waveguides. *Appl. Phys. B* **105**, 51 (2011).
- Large, N., Abb, M., Aizpurua, J. & Muskens, O. L. Photoconductively loaded plasmonic nanoantenna as building block for ultracompact optical switches. *Nano Lett.* **10**, 1741 (2010).
- Abb, M., Albella, P., Aizpurua, J. & Muskens, O. L. All-optical control of a single plasmonic nanoantenna-ITO hybrid. *Nano Lett.* **11**, 2457 (2011).
- Noskov, R. E., Krasnok, A. E. & Kivshar, Y. S. Nonlinear metal-dielectric nanoantennas for light switching and routing. *New J. Phys.* **14**, 093005 (2012).
- Zharov, A. A., Noskov, R. E. & Tsarev, M. V. Plasmon-induced terahertz radiation generation due to symmetry breaking in a nonlinear metallic nano dimer. *J. Appl. Phys.* **106**, 073104 (2009).
- Noskov, R. E., Zharov, A. A. & Tsarev, M. V. Generation of widely tunable continuous-wave terahertz radiation using a two-dimensional lattice of nonlinear metallic nanodimers. *Phys. Rev. B* **82**, 073404 (2010).
- Lapshina, N., Noskov, R. & Kivshar, Y. S. Nanoradar based on nonlinear dimer nanoantenna. *Opt. Lett.* **37**, 3921 (2012).
- Park, S. Y. & Stroud, D. Surface-plasmon dispersion relations in chains of metallic nanoparticles: An exact quasistatic calculation. *Phys. Rev. B* **69**, 125418 (2004).
- Johnson, P. B. & Christy, R. W. Optical constants of the noble metals. *Phys. Rev. B* **6**, 4370 (1972).
- Palpat, B. *inNon-Linear Optical Properties of Matter edited by Papadopoulos, M. G., Sadelj, A. J. & Leszczynski, J.* (Springer, Dordrecht, 2006) pp. 461–508.
- Rautian, S. G. Nonlinear saturation spectroscopy of the degenerate electron gas in spherical metallic particles. *JETP* **85**, 451 (1997).
- Drachev, V. P., Buin, A. K., Nakotte, H. & Shalae, V. M. Size dependent $\chi^{(3)}$ for conduction electrons in Ag nanoparticles. *Nano Lett.* **4**, 1535 (2004).
- Govyadinov, A. A., Panasyuk, G. Y., Schotland, J. C. & Markel, V. A. Theoretical and numerical investigation of the size-dependent optical effects in metal nanoparticles. *Phys. Rev. B* **84**, 155461 (2011).
- Weber, M. J. *Handbook of optical materials* (CRC Press, 2003).
- Palik, E. D. *ed. Handbook of Optical Constants of Solids* (Academic, Orlando, 1985).
- Chen, H., He, C., Wang, C., Lin, M., Mitsui, D., Eguchi, M., Teranishi, T. & Gwo, S. Far-field optical imaging of a linear array of coupled gold nanocubes: Direct visualization of dark plasmon propagating modes. *ACS Nano* **5**, 8223 (2011).
- Rosanov, N. N., Vysotina, N. V., Shatsev, A. N., Shadrivov, I. V. & Kivshar, Y. S. Hysteresis of switching waves and dissipative solitons in nonlinear magnetic metamaterials. *JETP Lett.* **93**, 743 (2011).



45. Rosanov, N. N., Vysotina, N. V., Shatsev, A. N., Shadrivov, I. V., Powell, D. A. & Kivshar, Y. S. Discrete dissipative localized modes in nonlinear magnetic metamaterials. *Opt. Express* **19**, 26500 (2011).
46. Torres-Torres, C., Peréa-López, N., Reyes-Esqueda, J. A., Rodríguez-Fernández, L., Crespo-Sosa, A., Cheang-Wong, J. C. & Oliver, A. Ablation and optical third-order nonlinearities in Ag nanoparticles. *Int. J. Nanomedicine* **5**, 925 (2010).
47. Rabinovich, M. I. & Trubetskov, D. I. *Oscillations and Waves in Linear and Nonlinear Systems* (Kluwer, Dordrecht, 1989).

Acknowledgements

This work was supported by the Ministry of Education and Science of Russia under the projects 11.G34.31.0020 and 14.B37.21.0942, and the Australian Research Council. The authors are indebted to A.A. Zharov and N.N. Rosanov for useful discussions.

Author contributions

R.N. and Y.K. suggested the idea. R.N. performed theoretical analysis and numerical simulations, wrote the first draft of the manuscript and prepared the figures and movies. P.B. contributed to the discussion of the results. Y.K. supervised the project and contributed to the manuscript preparation.

Additional information

Supplementary information accompanies this paper at <http://www.nature.com/scientificreports>

Competing financial interests: The authors declare no competing financial interests.

License: This work is licensed under a Creative Commons Attribution-NonCommercial-ShareAlike 3.0 Unported License. To view a copy of this license, visit <http://creativecommons.org/licenses/by-nc-sa/3.0/>

How to cite this article: Noskov, R. & Kivshar, Y. Oscillons, solitons, and domain walls in arrays of nonlinear plasmonic nanoparticles. *Sci. Rep.* **2**, 873; DOI:10.1038/srep00873 (2012).